

Cite this: *Nanoscale*, 2024, **16**, 9728

## Chemical passivation of 2D transition metal dichalcogenides: strategies, mechanisms, and prospects for optoelectronic applications

Zhaojun Li, <sup>\*a</sup> Hope Bretscher<sup>b</sup> and Akshay Rao<sup>c</sup>

The interest in obtaining high-quality monolayer transition metal dichalcogenides (TMDs) for optoelectronic device applications has been growing dramatically. However, the prevalence of defects and unwanted doping in these materials remain challenges, as they both limit optical properties and device performance. Surface chemical treatments of monolayer TMDs have been effective in improving their photoluminescence yield and charge transport properties. In this scenario, a systematic understanding of the underlying mechanism of chemical treatments will lead to a rational design of passivation strategies in future research, ultimately taking a step toward practical optoelectronic applications. We will therefore describe in this mini-review the strategies, progress, mechanisms, and prospects of chemical treatments to passivate and improve the optoelectronic properties of TMDs.

Received 10th December 2023,

Accepted 19th April 2024

DOI: 10.1039/d3nr06296a

rsc.li/nanoscale

### 1. Introduction

Since the successful exfoliation of monolayer graphene, research attention on various 2D materials has grown significantly.<sup>1–5</sup> Among 2D materials, transition metal dichalcogenides (TMDs), with the chemical structure  $MX_2$  ( $M = Mo, W$ ;  $X = S, Se, Te$ ), have been of great interest for optoelectronic applications due to their electronic and optical properties such as direct bandgaps, strong light–matter interactions, mechanical flexibility, and chemical and thermal stability to highlight a few.<sup>6–11</sup> Many proof-of-concept 2D TMD-based optoelectronic devices have been demonstrated.<sup>9,12–18</sup> However, in general, monolayer TMDs are imperfect and often contain various intrinsic and extrinsic defects.<sup>19</sup> Despite the remarkable potential of TMDs and the progress towards various optoelectronic applications, many challenges in improving their intrinsic qualities and limiting performance losses due to trion formation and defects persist.

In contrast to bulk TMD materials, excitons (electron–hole pairs) are strongly confined to the monolayer plane and also experience reduced screening due to the change in the dielectric environment.<sup>20</sup> A strong Coulomb interaction results in

tightly bound excitons with binding energies of several hundred meV, which dominate the optical and charge transport properties of 2D TMDs.<sup>21–23</sup> Quasiparticles, the so-called trions, formed by excitons and induced free charges through defects or adsorbates, have also been identified even at room temperature due to their strong electrostatic interactions and exhibit binding energies of tens of meV.<sup>24</sup> Background carrier concentrations can therefore play an important role in the recombination pathways and affect the optical and electronic properties of 2D TMDs. Additionally, oxygen and other adsorbates can alter the properties or degrade the qualities of 2D TMDs.<sup>25,26</sup> Substrate-supported TMD monolayers also suffer from strain variations introduced by the roughness of substrates, which modifies their electronic properties.<sup>27</sup> More importantly, due to their reduced dimensionality, 2D TMDs are predisposed to form atomic defects, such as vacancies, self-interstitials, grain boundaries, *etc.*<sup>19,28–32</sup> The electrons and holes in TMDs can be trapped in defect-resulting potentials, leading to localized excitons and non-radiative recombination pathways, which strongly influences the optical and electronic properties of TMDs.<sup>32–34</sup>

To this end, extensive efforts have been devoted to exploring approaches for preparing and improving the quality of semiconducting 2D TMD materials. The fact that 2D materials are essentially all surfaces provides a unique opportunity for controlling and tuning their optical and electronic properties. 2D TMD layers are extremely sensitive to all influences of the surrounding environment, and their properties can therefore be easily modified by external variables. Substrate engineering

<sup>a</sup>Solid State Physics, Department of Materials Science and Engineering, Uppsala University, 75103 Uppsala, Sweden. E-mail: zhaojun.li@angstrom.uu.se

<sup>b</sup>The Max Planck Institute for the Structure and Dynamics of Matter, 22761 Hamburg, Germany

<sup>c</sup>Cavendish Laboratory, University of Cambridge, JJ Thomson Avenue, CB3 0HE Cambridge, UK



like using a thin flake of hexagonal boron nitride (h-BN) as an interfacial layer reduces the structural damage and the associated interface states, which leads to cleaner optical and electronic properties.<sup>35–37</sup> Strain engineering has also emerged as a powerful strategy for tuning the optical bandgaps of TMD materials.<sup>38,39</sup> Phase engineering has been employed to enhance the electronic properties of TMDs.<sup>40,41</sup> Additionally, the surface chemical strategy, a versatile and non-destructive method, is one of the most effective approaches to tailor the properties of 2D TMD materials for practical device applications.<sup>42</sup> Compared to other approaches, chemical treatments are advantageous as they can be made compatible with other processing steps required for scaling-up device fabrication. However, designing treatments compatible with industry-scale device processing will require a precise understanding of the mechanisms behind known chemical treatments. Thus, setting up rational selection rules for chemicals to increase the potential of 2D TMDs in practical optoelectronic applications is of crucial importance. Previous review articles have discussed tuning optoelectronic properties by strain or substrate engineering and the observed effects of various chemical treatments.<sup>42–45</sup> However, to the best of our knowledge, no reviews addressed both the effects and mechanisms behind these effects of surface chemical treatments on 2D TMDs. To this end, this mini-review focuses on the recent efforts using various surface chemical treatments to achieve high quality optoelectronic applications, paying particular focus on the mechanisms behind such treatments.

In this mini-review, we start with an overview of the major studies over the past few years on chemical treatments that improve the semiconducting quality of 2D transition metal disulfides (TMDSS) including MoS<sub>2</sub> and WS<sub>2</sub> (Section 2). More specifically, Section 2.1 covers the characterization approaches of TMDs utilizing photoluminescence (PL) and electron mobility as the main quality indicators, as well as discrepancies among the reports in the literature, and Section 2.2 discusses the mechanisms of each chemical treatment including different proposed mechanisms. Given that the understanding of how several chemical treatments work has evolved over the past few years, we think the discussion of discrepancies between different works is important to clarify the chemical selection rules and guide the further design of chemical treatment strategies for defect passivation and property control. In Section 3, we will then turn our focus to the major studies and accompanying mechanisms of chemical treatments improving the quality of MoSe<sub>2</sub> and WSe<sub>2</sub>. In recent years, there have also been numerous studies on the preparation of high-quality 2D MoTe<sub>2</sub>, and it was theoretically predicted that Te vacancies can open a bandgap, which could be tuned by lattice strain or external forces.<sup>46,47</sup> However, little research has been done up to this point on chemical treatments of MoTe<sub>2</sub>, thus discussions of MoTe<sub>2</sub> and WTe<sub>2</sub> are not included in this mini-review.<sup>48</sup> Finally, we present our concluding remarks including issues addressed by chemical treatments, challenges facing the chemical treatment strategy development, and an outlook of future research directions in this area.

## 2. Chemical passivation of MoS<sub>2</sub> and WS<sub>2</sub>

The intrinsic doping of transition metal disulfides (TMDSS) may lead to the formation of positively or negatively charged excitons (trions) that redshift and broaden the PL spectra. Control of the carrier density is effective to modulate the optical properties of monolayer TMDs induced by the many-body bound effect.

Defects attenuate properties and device performance. In light-harvesting devices, defects can be detrimental if they assist carrier recombination and reduce mean free paths of carriers, consequently diminishing device performance. The predominant defect species and their percentages in 2D TMD monolayers synthesized *via* different methods or *via* mechanically exfoliated (ME) from bulk crystals will be different, and hence lead to different chemical treatment requirements. This might also be one of the factors that has caused discrepancy between the mechanisms disclosed in different studies. A large concentration of defects in ME MoS<sub>2</sub> monolayers observed in transmission electron microscopy (TEM) and scanning tunneling microscopy (STM) was thought to be sulfur vacancies (SVs) that possess the lowest formation energy, and in contrast to atom dislocations observed at the grain boundaries in chemical vapor deposition (CVD)-grown MoS<sub>2</sub>.<sup>49–51</sup> Hong *et al.* reported that antisite defects with Mo replacing the S atom are dominant point defects in physical vapour deposition (PVD)-grown ML MoS<sub>2</sub>, while SVs are predominant in ME and CVD-grown samples.<sup>49</sup> The defect density in the CVD-grown ML WS<sub>2</sub> interior is reported to be  $\sim 0.33 \text{ nm}^{-2}$  through atomically resolved scanning electron microscopy by Terrones and co-workers in 2017, which is four orders of magnitude higher than in mechanically exfoliated WS<sub>2</sub>.<sup>52</sup> In addition, the density of sulfur vacancies near the edges is around three times higher than in the interior in the CVD-grown WS<sub>2</sub>. Similar defect distribution in monolayer CVD-grown MoS<sub>2</sub> was reported by Schuck and co-workers.<sup>53</sup> On the other hand, Su *et al.* showed CVD-grown rhombic monolayer MoS<sub>2</sub> with PL intensity eight times stronger than CVD-grown triangular samples, indicating a low density of defects in rhombic monolayer MoS<sub>2</sub>. This was attributed to SV passivation by oxygen atoms which is predicted through density functional theory (DFT) simulations to remove in-gap states.<sup>54</sup> Moreover, there is still debate on the origin of defects existing in TMDs. A previous study has shown that oxygen substitutions can be the dominant defects instead of sulfur vacancies and that differentiating between them is not possible using high-resolution TEM alone.<sup>55</sup> Therefore, we have carefully included synthesis methods of TMDs for different chemical passivation studies.

### 2.1 Characterization

**2.1.1 Photoluminescence enhancement.** The PL intensity or photoluminescence quantum yield (PLQY) serves as a quality indicator of 2D TMDs for optoelectronic applications as it is sensitive to many-body effects, defects, and sub-



bandgap states.<sup>56–58</sup> The structures of reported chemicals which led to PL enhancements are summarized in Fig. 1. Matsuda and co-workers reported the exciton PL enhancement of mechanically exfoliated (ME) MoS<sub>2</sub> by drop-casting p-type chemical dopants 2,3,5,6-tetrafluoro-7,7,8,8-tetracyanoquinodimethane (F4TCNQ) and 7,7,8,8-tetracyanoquinodimethane (TCNQ).<sup>59,60</sup> Su *et al.* showed substantial PL intensity enhancement of ME monolayer MoS<sub>2</sub> through the physisorption of H<sub>2</sub>O<sub>2</sub> as a p-dopant.<sup>61</sup> Tongay *et al.* reported over 100 times improvement in the PL intensity of ME monolayer MoS<sub>2</sub> by physical adsorption of electronegative molecules like O<sub>2</sub> and H<sub>2</sub>O.<sup>62</sup> The authors also illustrated that the charge transfer from MoS<sub>2</sub> to O<sub>2</sub> reduced the original sheet carrier density of MoS<sub>2</sub> as much as 0.5 nm<sup>-2</sup> assuming that one O<sub>2</sub> molecule was physisorbed on each unit cell of MoS<sub>2</sub> *via* DFT calculations. Similar results were obtained by Peimyoo *et al.* through drop-casting F4TCNQ and H<sub>2</sub>O on ME monolayer WS<sub>2</sub> and by Nan *et al.* through high-temperature annealing ME monolayer MoS<sub>2</sub> due to O<sub>2</sub> bonding (Fig. 2a–d).<sup>63,64</sup> As shown in Fig. 3, the reduction redox of these molecules lies below the conduction band minima (CBM) of MoS<sub>2</sub> and WS<sub>2</sub>, so charges can be depleted from intrinsically n-doped MoS<sub>2</sub> and WS<sub>2</sub>. The p-doping effect was evidenced by the blue-shifted PL spectra, a more positive threshold voltage of back-gated TMD FETs, and a red-shifted out-of-plane vibration (A<sub>1g</sub>) peak in Raman spectra.<sup>63,64</sup> Sun *et al.* reported higher PL intensity in CVD-grown MoS<sub>2</sub> monolayers as compared to ME MoS<sub>2</sub> monolayers,

which was attributed to the high p-doping effect of adsorbates in air.<sup>65</sup> Similarly, Xu *et al.* observed that the PL intensity of thermal vapor sulfurized (TVS) monolayer MoS<sub>2</sub> synthesized in a vacuum was significantly attenuated relative to TVS monolayer MoS<sub>2</sub> synthesized in air and proposed that the higher PL intensity of MoS<sub>2</sub> in air was facilitated by molecular adsorption (O<sub>2</sub>, N<sub>2</sub>, etc.) on SVs.<sup>66</sup>

In 2015, Javey and co-workers demonstrated a near-unity PLQY with no change in the overall spectral shape for ME MoS<sub>2</sub> monolayers on oxide substrates through a chemical treatment by the nonoxidizing organic superacid bis-(trifluoromethane)sulfonimide (H-TFSI).<sup>67</sup> They also observed that the PL lifetime of MoS<sub>2</sub> was lengthened from roughly 250 ps to 10 ns after the H-TFSI treatment. Later on, Javey and co-workers reported an encapsulation approach with an amorphous fluoropolymer CYTOP and a subsequent H-TFSI treatment, which yielded a near-unity PLQY in both ME MoS<sub>2</sub> and WS<sub>2</sub> monolayers with excellent stability against post-processing.<sup>68</sup> They proposed that the strong protonating nature of the superacid removed the contaminants on the surface and suppressed defect-mediated nonradiative recombination in the monolayers. Goodman *et al.* reported that the deep trapped dark exciton states which were associated with native structural defects were responsible for the long PL lifetime of H-TFSI-treated MoS<sub>2</sub>, and the H-TFSI treatment reduced nonradiative recombination through these states.<sup>69</sup> The exact mechanism of H-TFSI treatment is, however, not fully understood, which has been investigated by a few research groups. This will be further discussed in detail in Section 2.2.

In 2017, Atallah *et al.* reported that charged defects in CVD-grown MoS<sub>2</sub> monolayers could be electrostatically passivated by ionic liquids (ILs) with a grounded metal contact, leading to up to two orders of magnitude increase in the PL yield.<sup>70</sup> Similarly, Park *et al.* showed PL enhancement and defect passivation of CVD-grown ML MoS<sub>2</sub> with a ML of titanyl phthalocyanine (TiOPc).<sup>71</sup> Poly(3,4-ethylenedioxythiophene) polystyrene sulfonate (PEDOT:PSS) was reported to passivate the SVs in CVD-grown MoS<sub>2</sub> by a sulfur adatom cluster through a hydrogenation process confirmed by the high-angle annular-dark-field (HAADF) scanning transmission electron microscopy (STEM) images (Fig. 2e–h) and X-ray photoelectron spectroscopy (XPS) measurements.<sup>72</sup> In that study, a high-performance lateral monolayer MoS<sub>2</sub> homojunction with an excellent photoresponsivity of ~308 mA W<sup>-1</sup> and outstanding air stability after two months was achieved employing that strategy. In that study, the electron concentration of MoS<sub>2</sub> after the treatment decreased by 643 times, and led to a work function increase of ~150 meV and an enhanced PL intensity. Jin and co-workers demonstrated the passivation of SVs in both CVD-grown and ME MoS<sub>2</sub> monolayers *via* various thiol molecules, which led to an enhanced PL intensity.<sup>73</sup> The authors used thiol molecules with F-containing ligands as markers, and the functionalized products were characterized with XPS and Fourier transform infrared (FTIR) spectroscopy (Fig. 2i and j). The reported mechanism of this chemical treatment is discussed in Section 2.2.2. Yao *et al.* immersed a CVD-grown WS<sub>2</sub>

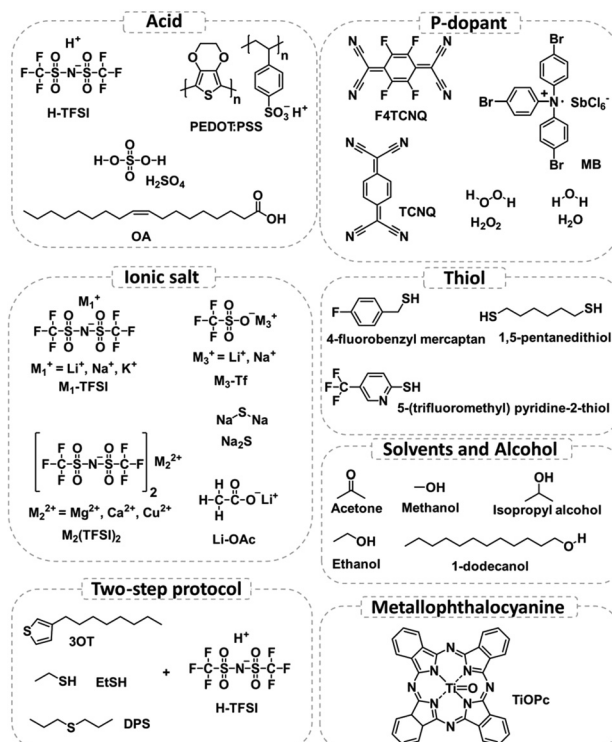
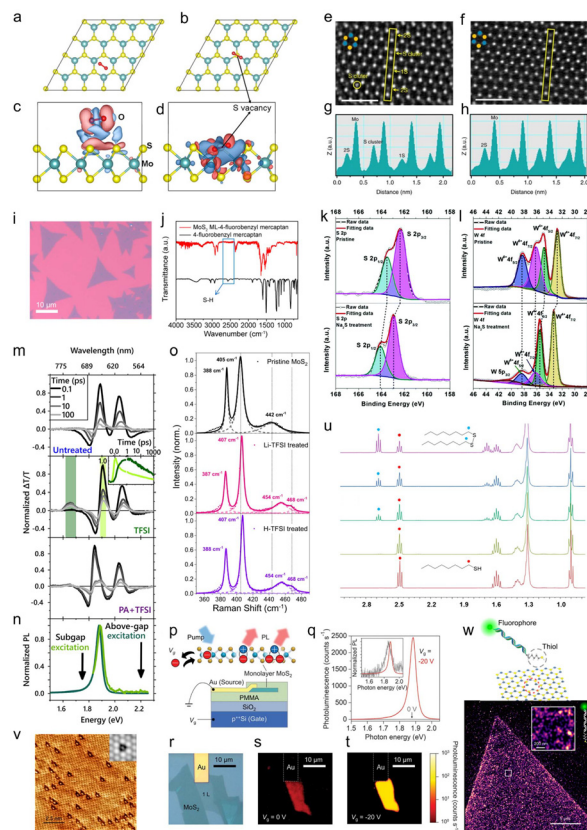
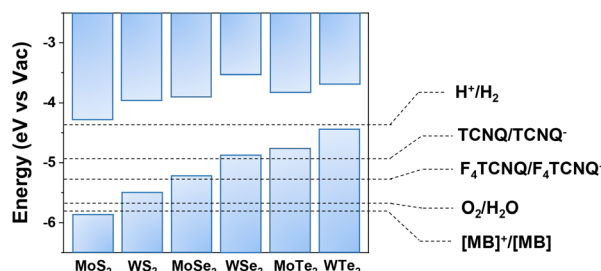


Fig. 1 Structures of chemicals used in previous studies for the PL enhancement of 2D TMDs. This figure has been adapted from ref. 94 with permission from Springer Nature, copyright 2021.





**Fig. 2** Summary of varied techniques employed to illustrate the chemical treatment mechanisms. DFT simulation on the adsorption of O<sub>2</sub> on the 2D MoS<sub>2</sub> surface. Relaxed configuration and charge density difference of an O<sub>2</sub> molecule physisorbed on perfect monolayer MoS<sub>2</sub> (a and c) and chemisorbed on defective monolayer MoS<sub>2</sub> containing a monosulfur vacancy (b and d). The positive and negative charges are shown in red and blue, respectively. Reproduced from ref. 64 with permission from American Chemical Society, copyright 2014. (e–h) PSS-induced SVSH mechanism supported by HAADF STEM images. HAADF images obtained before (e) and after (f) PSS-induced SVSH, together with the Z-contrast mapping obtained before (g) and after (h) PSS-induced SVSH in the areas marked with yellow rectangles, revealing that the SVs (1S) are healed spontaneously by the sulfur adatom clusters on the MoS<sub>2</sub> surface through a PSS-induced hydrogenation process. The cyan and yellow dots indicate the Mo and S atoms, respectively. Scale bar, 1 nm. Adopted from ref. 72 with permission from Springer Nature, copyright 2017. (i and j) Functionalization of the CVD-grown MoS<sub>2</sub> monolayer with thiol molecules supported by FTIR measurement. (i) Typical optical microscopy image of CVD-grown MoS<sub>2</sub> monolayers on a sapphire substrate. (j) FTIR spectra of 4-fluorobenzyl mercaptan-functionalized MoS<sub>2</sub> MLs (red) in comparison with those of the free 4-fluorobenzyl mercaptan ligand (black). Reproduced from ref. 73 with permission from American Chemical Society, copyright 2014. (k and l) High-resolution XPS spectra of S 2p and (l) XPS spectra of W 4f before and after chemical treatment with Na<sub>2</sub>S solution (0.05 M). Reproduced from ref. 74 with permission from the Royal Society of Chemistry, copyright 2018. (m and n) Defect passivation of ME MoS<sub>2</sub> supported by optical spectroscopy techniques. (m) Pump–probe spectra of MoS<sub>2</sub> untreated (top), H-TFSI-treated (middle), and thiol + H-TFSI-treated (bottom) MoS<sub>2</sub>. H-TFSI treatment results in a prominent sub-gap bleach associated with sulfur vacancy defects. The inset shows the normalized kinetics taken at the A exciton bleach (light green) and defect peak (dark green) in the TFSI-treated sample, illustrating the transfer from the band edge to the sub-gap defect state. (n) PL emission with sub-gap excitation of H-TFSI-treated MoS<sub>2</sub> occurs at the same energy as PL emitted by the above-bandgap excitation of H-TFSI-treated MoS<sub>2</sub>. Reproduced from ref. 83 with permission from American Chemical Society, copyright 2021, licensed under CC-BY 4.0. (o) Chemical adsorption supported by Raman measurements. Raman spectra of untreated, H-TFSI-treated, and Li-TFSI-treated monolayer MoS<sub>2</sub>. The decomposed Lorentzian peak fitting of each spectrum is presented as a short, dashed line and the cumulative fitting is presented as a solid line. The positions of A<sub>1g</sub> and 2LA modes of untreated MoS<sub>2</sub> and the A<sub>2u</sub> mode of MoS<sub>2</sub> with an adatom (Li, for example) are illustrated in each spectrum with a short black dashed line for direct comparison. The value of each peak position is also stated in the spectra. Reproduced from ref. 94 with permission from Springer Nature, copyright 2021. (p–t) Schematics of the device and the gate dependence of photoluminescence in MoS<sub>2</sub>. (p) Schematic showing control of different quasiparticles by the gate voltage V<sub>g</sub> and generation rate G. (q) PL spectra of the MoS<sub>2</sub> monolayer device under gate voltages of V<sub>g</sub> = –20 and 0 V at a generation rate of G = 10<sup>18</sup> cm<sup>–2</sup> s<sup>–1</sup>. Inset: normalized PL spectra. (r) Top-view optical micrograph of a MoS<sub>2</sub> device. (s and t) PL images of the device at (r) V<sub>g</sub> = 0 V and (s) V<sub>g</sub> = –20 V. Reproduced from ref. 103 with permission from AAAS, copyright 2019. (u) <sup>1</sup>H NMR (400 MHz, CD<sub>3</sub>OD) spectra of pure 1-octanethiol after heating 1-octanethiol in CD<sub>3</sub>OD under reflux (in air) for 24 h and a 1-octanethiol/exfoliated 2H-MoS<sub>2</sub> reaction mixture (in air) after 4 h, 6 h, and 24 h (from top to bottom). Highlighted triplet resonances: 1-octanethiol, δ = 2.49 ppm, red dot; dioctyl disulfide, δ = 2.68 ppm, blue dot. Other signals are associated with either 1-octanethiol or the disulfide derivative thereof. Reproduced from ref. 113 with permission from American Chemical Society, copyright 2018. (v) Higher-resolution STM image displaying the incorporation of O atoms (bright spots) into S vacancies (dark triangles). Inset: simulated STM image based on DFT calculations of an O-saturated S vacancy site in the 2D MoS<sub>2</sub> crystals. Reproduced from ref. 118 with permission from Springer Nature, copyright 2018. (w) 2D-PAINT image acquired using fluorescent probes consisting of a fluorophore head, dsDNA of 70 bp as a linker molecule, and a thiol tail (FAM-dsDNA70bp-SH). The zoomed-in image reveals a high density of binding on MoS<sub>2</sub>. Reproduced from ref. 115 with permission from American Chemical Society, copyright 2021, licensed under CC-BY-NC-ND 4.0.



**Fig. 3** Calculated band alignment of  $\text{MoS}_2$ ,  $\text{WS}_2$ ,  $\text{MoSe}_2$ ,  $\text{WSe}_2$ ,  $\text{MoTe}_2$ , and  $\text{WTe}_2$  along with electrochemical redox potentials of the p-dopants from the literature. This figure has been adapted from ref. 42 with permission from the Royal Society of Chemistry, copyright 2018.

monolayer into sodium sulfide ( $\text{Na}_2\text{S}$ ) solution and achieved enhanced PL emission with  $\text{WO}_{3-x}$  defect passivation validated by XPS measurements (Fig. 2k and l).<sup>74</sup> In their study, the inhomogeneous PL emission in the inner and edge regions of the pristine  $\text{WS}_2$  monolayer was attributed to the different charge populations and defect states across the monolayer area, which was clarified by the STEM images showing both SVs and W vacancies. The authors also observed a redshift of the PL spectra of ML  $\text{WS}_2$  after the  $\text{Na}_2\text{S}$  treatment, which was due to the increased formation of trions and biexcitons evidenced by steady-state low temperature and laser power-dependent PL measurements.<sup>74</sup> Recently, Zhang and co-workers reported that the PLQY of  $\text{MoS}_2$  quantum sheets produced by silica-assisted ball milling (BE) and sonication-assisted solvent exfoliation was enhanced to 18.5% *via* a heat treatment method based on the polar solvent tetrahydrofuran (THF).<sup>75</sup> They showed increased radiative relaxation by time-resolved PL (TRPL) measurements and their XPS and high resolution transmission electron microscopy (HRTEM) results suggested that S and Mo formed an oxidized state and the passivation/deformation was from the edge inwards.

**2.1.2 Mobility improvement.** Mobility serves as another quality indicator of 2D TMDs for optoelectronic applications, which is sensitive to charged impurities, traps, and structural defects both inside the material and at the dielectric interface due to their atomic thickness. Interface engineering like the use of crystalline h-BN and thiol-terminated  $\text{SiO}_2$  substrates was found to effectively improve the device mobility by suppressing the extrinsic scattering process and modifying the properties of TMDs.<sup>76,77</sup> N-doping like using hydrazine on the surface of  $\text{MoS}_2$  flakes to increase the density of carriers also led to an increased mobility of TMDs.<sup>78</sup> Radisavljevic *et al.* realized a mobility of  $\sim 200 \text{ cm}^2 \text{ V}^{-1} \text{ s}^{-1}$  in an FET with an ME  $\text{MoS}_2$  monolayer as a conductive channel and  $\text{HfO}_2$  as a gate insulator.<sup>79</sup> In 2014, Yu *et al.* reported a high mobility  $> 80 \text{ cm}^2 \text{ V}^{-1} \text{ s}^{-1}$  in a backgated (3-mercaptopropyl)trimethoxysilane (MPS)-treated ME  $\text{MoS}_2$  FET at room temperature with SV passivation, revealing the potential of chemical treatments for achieving intrinsic charge transport of 2D TMDs.<sup>80</sup> The mechanism of MPS treatment is addressed in Section 2.2.2 together with other defect passivation approaches. In 2017, Neupane

*et al.* demonstrated a carrier mobility increase of both ME and CVD-grown TMDS monolayer-based FETs *via* methanol treatment.<sup>81</sup> They observed a concomitant enhancement in the PL spectral weights of trions, a redshift of the Raman  $\text{A}_{1g}$  mode, and upshifted peaks in the XPS spectra of TMD monolayers after the methanol treatment, which confirmed the n-doping effect. The authors also proposed that methanol contributed to the reduction of defects in TMD materials validated by the increased exciton absorption peaks and prolonged fluorescence lifetime of TMD monolayers after the methanol treatment.<sup>81</sup>

In 2019, Rao and co-workers reported a greatly enhanced PL intensity of ME  $\text{WS}_2$  monolayers *via* oleic acid (OA, shown in Fig. 1) treatment comparable to that of H-TFSI-treated monolayers, and simultaneously improved the mobility in  $\text{WS}_2$ -based FET devices due to defect passivation.<sup>82</sup> Later, they reported a generalizable SV passivation protocol using a passivating agent (thiol, thiophene, or sulfide, Fig. 1), followed by the H-TFSI treatment. This two-step chemical treatment simultaneously achieved improved mobility and an increase in the PL intensity of both  $\text{MoS}_2$  and  $\text{WS}_2$  monolayers.<sup>83</sup> The detailed mechanism of this chemical treatment is discussed together with the H-TFSI treatment in Section 2.2.1. In 2021, Samori and co-workers used  $\pi$ -conjugated dithiolated molecules to bridge adjacent  $\text{MS}_2$  flakes produced by liquid exfoliation. This led to an enhanced field-effect mobility ( $\sim 10^{-2} \text{ cm}^2 \text{ V}^{-1} \text{ s}^{-1}$ ) and  $I_{\text{ON}}/I_{\text{OFF}} (\sim 10^4)$ , along with the fastest switching time ( $\sim 18 \text{ ms}$ ), showing the importance of chemical treatment for the development of high-performance and printed electronics based on solution-processed TMDs.<sup>84,85</sup>

**2.1.3 Discrepancy.** Even though defect passivation in 2D TMDSS was often correlated with PL enhancement as stated in Section 2.1.1, there were also chemical treatments reported that led to defect passivation without PL enhancement. Nguyen *et al.* investigated the effect of chemical treatments on the electronic structure of liquid phase exfoliated (LPE)  $\text{MoS}_2$  nanosheets *via* a series of thiols. The studied chemicals were thiols with aromatic rings of different electron-withdrawing capabilities and alkylthiols with different chain lengths. The authors observed redshifted PL spectra after chemical treatments without significant changes in decay kinetics and attributed these phenomena to the formation of shallow trap states upon functionalization through the defect sites of  $\text{MoS}_2$ .<sup>86</sup> In their report, the successful thiolation on the surface of  $\text{MoS}_2$ , resulting in cathodic valence and conduction band edge shifts of  $\sim 500 \text{ meV}$ , was confirmed by both ATR-IR and XPS measurements. Pierucci *et al.* reported that the incorporation of atomic hydrogen in the CVD-grown  $\text{MoS}_2$  monolayer could saturate the SVs forming Mo-H bonds and preserve the well-defined electronic structure of the  $\text{MoS}_2$  monolayer evidenced by high-resolution XPS measurements and DFT calculations.<sup>87</sup> However, they observed a decrease in PL intensity after hydrogenation which was explained by the suppression of PL originated by defects from  $\text{MoS}_2$ . The varied impact on the PL intensity of TMDs caused by different defect passivation chemicals could also be ascribed to the opposite (n *vs.* p)

doping effect of the chemicals. Jung and co-workers reported the SV passivation on ME 4-layer MoS<sub>2</sub> with two thiol molecules: mercaptoethylamine with lone electron pairs served as an n-dopant leading to a decrease in the PL intensity of MoS<sub>2</sub> after the treatment, while 1H,1H,2H,2H-perfluorodecanethiol caused a p-doping effect and resulted in an enhancement in the PL intensity of MoS<sub>2</sub> after the treatment.<sup>88</sup> Moreover, Amsterdam *et al.* illustrated that the deposition of metallophthalocyanines (MPcs) on ME monolayer MoS<sub>2</sub> quenched the low-temperature defect PL, with the quenching efficiency decreasing in the order CoPc > CuPc > ZnPc.<sup>89</sup> The authors observed partial PL quenching of the MoS<sub>2</sub> A-exciton peak after MPcs deposition, which was ascribed to the mutual charge transfer *via* the formation of a type II heterojunction.

## 2.2 Mechanisms of chemical treatments

**2.2.1 Mechanisms of chemical treatments without defect passivation.** P-type doping is the most common mechanism of chemical treatments presented since monolayer MoS<sub>2</sub> and WS<sub>2</sub> are intrinsically n-doped. Trions emit at longer wavelengths with an emission efficiency much lower than that of neutral excitons.<sup>35</sup> The charge transfer between the dopant and the 2D TMD material modulates the Fermi levels of the TMDs and results in the modification of the optical and electronic properties of TMD monolayers.<sup>90</sup> For 2D TMDs, P-doping promotes the emission of neutral excitons over trions, leading to an enhancement and blueshift in PL, while the defect states and basic electronic structures of the TMD material remain unaltered. The chemical structures of p-dopants reported and their electrochemical redox potentials, as well as the calculated band alignment of 2D TMDs, are summarized in Fig. 1 and 2, respectively. Zhang *et al.* investigated the doping effect on ME MoS<sub>2</sub>, WS<sub>2</sub>, MoSe<sub>2</sub>, and WSe<sub>2</sub> monolayers with “Magic Blue” [N(C<sub>6</sub>H<sub>4</sub>-p-Br)<sub>3</sub>]SbCl<sub>6</sub> as the p-dopant, and achieved PL enhancement for all four TMD materials.<sup>91</sup> The extent of the doping level was modified by varying the concentration of dopant solutions and treatment time, and the authors confirmed the doping effect by transistor measurements and PL, Raman, and XPS spectroscopy. Birmingham *et al.* reported the effect of dopant phases (liquid or gaseous) on the PL intensity of the CVD-grown MoS<sub>2</sub> monolayer *via* *in situ* Raman microspectroscopy and concluded that the liquid dopant contributed to lower charge transfer efficiency.<sup>92</sup> Wang *et al.* revealed that the effect of p-type doping on 2D TMDs not only depended on the chemical potential difference between the dopants and TMD materials, but also on the thermodynamic stability of physisorption by means of temperature-dependent PL measurements, gate-induced PL measurements and DFT calculations.<sup>93</sup> Rao and co-workers compared the effect of various chemical treatments including a series of ionic chemicals, H-TFSI, and small molecule p-dopants on the optical properties of monolayer TMDs and demonstrated that ionic salts like Li-TFSI, which are compatible with a range of green solvents, enhanced the PL intensity of both ME MoS<sub>2</sub> and WS<sub>2</sub> monolayers to a level double that of H-TFSI treatment.<sup>94</sup> The authors revealed that both cations and counter anions play

important roles in enhancing the PL intensity of TMDs. The cations must be stably adsorbed on the TMD surfaces and the counter anions should be non-coordinating with strong electron-withdrawing groups. Their conclusions were supported by the appearance of the A<sub>2u</sub> mode in Raman spectra (Fig. 2o), cation adsorption *via* DFT simulation, and TRPL and PL diffusion measurements.<sup>94</sup> Recently, Zhou and co-workers demonstrated a universal p-type doping with Lewis acid SnCl<sub>4</sub> *via* Sn<sup>4+</sup> ion exchange for TMDs, which is also proved by DFT calculations.<sup>95</sup>

Cation intercalation has been proposed as another mechanism of chemical treatments. The intercalated cations can result in p-type doping to the monolayer TMDs and reduce the substrate influence simultaneously. In 2017, Yu *et al.* demonstrated that the PL of the CVD as-grown and transferred WS<sub>2</sub> monolayer was enhanced due to the intercalation of small cations (H<sup>+</sup> and Li<sup>+</sup>) between the monolayers and underlying substrates, which was achieved by simply immersing substrate-supported monolayers into a certain chemical solution.<sup>96</sup> The intercalation was evidenced by an increase in the atomic force microscopy (AFM)-measured height of the as-grown monolayers after the chemical treatment. Through a series of steady-state PL measurements, they also concluded that intercalation was less likely to occur in TMD monolayers that interacted with substrates more strongly, like for the as-grown monolayers or monolayers on 2D material substrates (h-BN, for example).

The mechanism of H-TFSI treatment is a topic of specific focus since this chemical treatment has received the most attention in the past few years following the report of Javey and co-workers. In 2017, Kim and co-workers found that the H-TFSI treatment had a minimal effect on the inner region of triangular CVD-grown WS<sub>2</sub> monolayers, whereas the PL of WS<sub>2</sub> in the edge regions was enhanced up to 25 times.<sup>97</sup> They concluded that H-TFSI p-doped the sample, and reduced defects which they assumed were distributed unequally throughout the sample, thus leading to spatially heterogeneous effects. Subsequently, Kim and co-workers reported that SVs in CVD-grown MoS<sub>2</sub> were directly repaired by the extrinsic sulfur atoms produced from the dissociation of H-TFSI, evidenced through a correlative combination of optical characterization, atomic-scale STEM, and DFT calculations.<sup>98</sup> The detailed mechanism of the H-TFSI treatment proposed by the authors is shown in Fig. 4a, where the H-TFSI molecule initially released SO<sub>2</sub>, after which a SV was passivated, resulting in the dissociation of an O<sub>2</sub> molecule from the SO<sub>2</sub> after SV passivation. The authors also observed that the PL peak position of MoS<sub>2</sub> blueshifted by ~5 nm and the A<sub>1g</sub> Raman mode blueshifted by 0.6 cm<sup>-1</sup> after the H-TFSI treatment, suggesting a p-type doping effect. On the other hand, Kiriya *et al.* compared the effect of H-TFSI treatments in various solvents on the PL intensity of the ME MoS<sub>2</sub> monolayer with H<sub>2</sub>SO<sub>4</sub> and Li<sub>2</sub>SO<sub>4</sub> in water and concluded that the proton is a key factor in enhancing the PL intensity of MoS<sub>2</sub>.<sup>99</sup> Relatedly, Lu *et al.* reported that the effectiveness of H-TFSI depended critically on the charge state and protons donated by H-TFSI.<sup>100</sup> According to



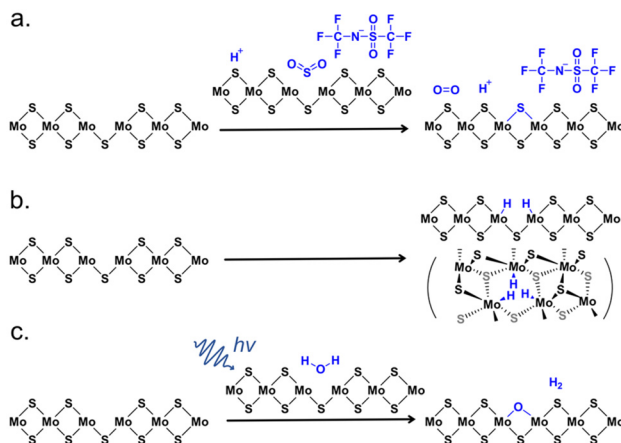


**Fig. 4** Reported mechanisms behind H-TFSI and H<sub>2</sub>O treatments for monolayer MoS<sub>2</sub> defect passivation. (a) Illustration of the reaction between H-TFSI and monolayer MoS<sub>2</sub> through the SV sites. (b) Illustration of the interaction between H-TFSI and monolayer MoS<sub>2</sub> through the SV sites. (c) Illustration of photon-mediated passivation with a H<sub>2</sub>O molecule on the surface of MoS<sub>2</sub>. Adapted from ref. 121 with permission from American Chemical Society, copyright 2019.

their DFT simulations, three H atoms symmetrically adsorbed around the SV site in its  $-1$  charge state, which could remove all gap states (Fig. 4b). Schwermann *et al.* revealed through first-principles calculations that H-TFSI transferred oxygen to the surface of monolayer MoS<sub>2</sub>, yielding a defect-free electronic band structure like that of pristine MoS<sub>2</sub>.<sup>101</sup> The authors also pointed out that there were similar reactions with H<sub>2</sub>O<sub>2</sub>, O<sub>2</sub>, and H<sub>2</sub>SO<sub>4</sub> (but not H<sub>2</sub>O) treatments, which was supported by simulations and steady-state PL measurements. Molas *et al.* observed that the H-TFSI treatment resulted in progressive quenching of defect-related emission in ME MoS<sub>2</sub> monolayers at low temperatures, again concluding the defect-passivating effect of H-TFSI treatment.<sup>102</sup>

Countering the growing body of claims that H-TFSI passivates defects through some mechanisms, in 2019, Javey and co-workers showed a near-unity PL QY of pristine ME MoS<sub>2</sub> and WS<sub>2</sub> monolayers through electrostatic doping and revealed that the underlying mechanism of the H-TFSI treatment is p-type doping without defect passivation further justified by the TRPL measurements, where the H-TFSI treatment led to similar decay kinetics compared to electrostatic doping (Fig. 2p-t).<sup>103</sup> Their work implied that all neutral excitons in 2D TMDSS radiatively recombined even in the presence of native defects. On the other hand, Pain and co-workers reported the PL enhancement of 2D TMDSS with superacid analogues and pointed out that acidity and the inclusion of sulfur and oxygen from H-TFSI did not necessarily play roles in defect passivation.<sup>104</sup> Rao and co-workers observed a much longer PL lifetime (1–20 ns) upon H-TFSI treatment compared to the ME pristine MoS<sub>2</sub> monolayer which fell below the instrument response of 100 ps, indicating a trap-mediated exciton recombination process after the H-TFSI treatment.<sup>83</sup> In addition, the authors experimentally observed sub-gap trap

sites (originating from SVs) in H-TFSI-treated MoS<sub>2</sub>, which appeared as a positive feature at 730 nm in ultrafast pump-probe spectra. This sub-gap defect bleach grew simultaneously with the initial A exciton decay, confirming a transfer in population from the A excitons to the defect states. They also reported a decrease in carrier mobility by over two orders of magnitude in H-TFSI-treated FETs compared to untreated devices. The authors concluded that even though H-TFSI treatment increased the PLQY, the SVs were still present and significantly limited the quality of the TMD material. In addition, they have conducted a two-step chemical treatment, a passivating agent (thiol, thiophene, or sulfide) followed by the H-TFSI treatment, which achieved an enhanced PL intensity and shortened emission lifetime compared to the H-TFSI-treated-only sample.<sup>83</sup> In contrast to the H-TFSI-only treatment, the sub-gap bleach was greatly reduced in the two-step treatment, suggesting the passivation of SV sites (Fig. 2m and n). The understanding of the mechanism behind H-TFSI treatment is then the key to further designing chemical treatments to passivate the defects of 2D TMDs.

**2.2.2 Mechanisms of chemical treatments with defect passivation.** Defect passivation is defined as a process that removes the defect states from the energy gap between the valence and conduction bands without shifting the Fermi energy ( $E_F$ ) into either band. At the time of writing this review, more investigations are required to identify the exact mechanism by which structural defects are repaired in TMD materials, as multiple proposals currently have been put forward in the literature. A few groups reported that SVs in MoS<sub>2</sub> and WS<sub>2</sub> monolayers were chemically acting as catalytic sites for hydrodesulfurization reactions and, therefore, could be passivated. This was proposed as the sulfur vacancy self-healing (SVSH) mechanism.<sup>105,106</sup> Yu *et al.* reported the reaction kinetics between the MPS molecule and MoS<sub>2</sub> simulated with DFT calculations.<sup>80</sup> As shown in Fig. 5a, the MPS molecule was chemically absorbed on the SV site of the MoS<sub>2</sub> surface by cleaving the S-H bond. It formed a thiolate intermediate and the dissociated H atom bonded to a neighboring S atom. Then the S-C bond cleaved and formed the final product, trimethoxy(propyl)silane, after hydrogenation. The S-C bond in MPS was found to be weaker than other alkylthiol molecules due to the acidic nature of CH<sub>3</sub>-O<sup>-</sup> groups which led to a low energy barrier for the reaction. In addition, the authors proposed that the (CH<sub>3</sub>O)<sub>3</sub>-Si- groups reacted with the SiO<sub>2</sub> substrate to form a self-assembled monolayer which passivated the MoS<sub>2</sub>/SiO<sub>2</sub> interface. A similar mechanism was reported by Zhang *et al.* where the electrically neutral S adatoms filled the SVs of the CVD-grown MoS<sub>2</sub> monolayer through a poly(4-styrenesulfonate) (PSS)-induced hydrogenation process in a mildly acidic PEDOT:PSS environment.<sup>72,107</sup> This finding was supported by both STEM and XPS measurements which showed that the contribution of the intrinsic MoS<sub>2</sub> species in the XPS spectra increased after the treatment.

The SV passivation with thiol chemistry has also been explored by multiple groups, yet both the resulting products and reaction mechanisms remain controversial. One reported

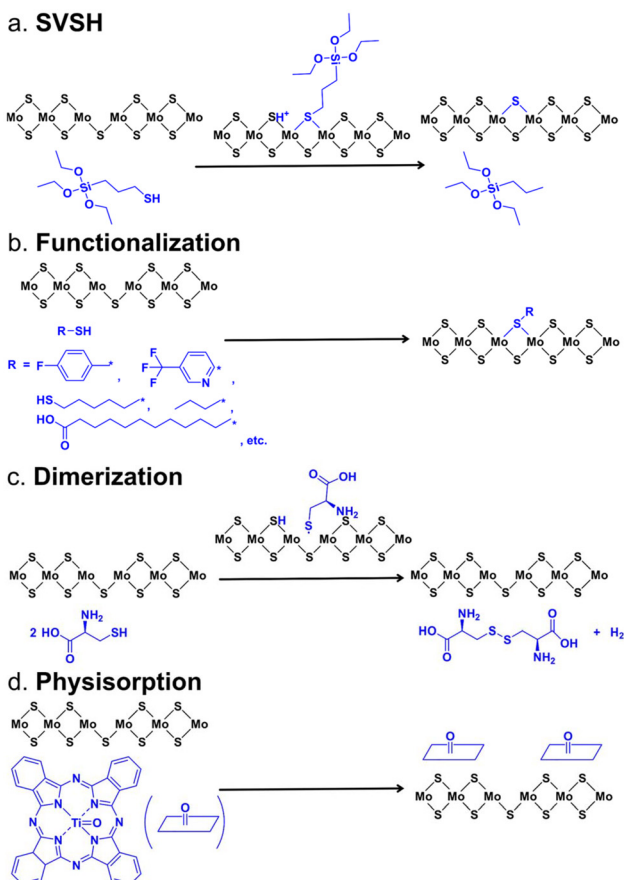


**Fig. 5** Schematics of the reaction kinetics that have been reported for passivating the SVs. (a) Reaction between the MPS molecules and monolayer  $\text{MoS}_2$  through the sulfur vacancy self-healing (SVSH) mechanism. (b) Reaction between various thiol molecules and monolayer  $\text{MoS}_2$  through the functionalization mechanism. (c) Reaction between the thiol molecule and monolayer  $\text{MoS}_2$  through the dimerization mechanism. (d) Interaction between the TiOPc molecule and monolayer  $\text{MoS}_2$  through the physisorption mechanism.

mechanism of SV passivation is that thiol molecules conjugated to the TMD surface with the S-H bond cleaved rather than physisorption or chemisorption, as illustrated in Fig. 5b.<sup>73,86,108–110</sup> This was proposed as the functionalization mechanism and was often visualized by FTIR measurements in which the S-H band from thiol molecules was found at  $2563\text{ cm}^{-1}$ , but absent after conjugation with  $\text{MoS}_2$ . Similarly, Cho *et al.* reported that alkanethiol molecules passivated the SVs through chemisorption at the SV sites of few-layer  $\text{MoS}_2$ , evidenced by a shift of the characteristic peak position in XPS after the treatment.<sup>111</sup> On the other hand, McDonald and co-workers proposed that TMDs facilitated the oxidation of organic thiols to disulfides, which were physisorbed on the 2D TMD surfaces through electrostatic interactions, rather than coordinate at SVs.<sup>112</sup> This was proposed as the dimerization mechanism. The disulfide products were evidenced by diffuse reflectance infrared Fourier transform (DRIFT) measurements. In this scenario, thiols initially donated a hydrogen atom to the TMD. The formed thyl radicals yielded disulfides and the

$\text{H}[\text{MoS}_2]$  released hydrogen gas. The proposed mechanism is illustrated in Fig. 5c. Subsequently, McDonald and co-workers quantitatively monitored the consumption of 1-octanethiol in the presence of liquid exfoliated  $\text{MoS}_2$  nanosheets using  $^1\text{H}$  nuclear magnetic resonance (NMR) spectroscopy and further confirmed the dimerization mechanism they proposed previously where  $\text{MoS}_2$  facilitated the oxidation of thiols to disulfides (Fig. 2u).<sup>113</sup> In 2017, Wang and co-workers investigated the reaction mechanisms between the defective  $\text{MoS}_2$  monolayer and thiol molecules employing potential energy surface calculations and kinetic studies.<sup>114</sup> They concluded that the reactions were dominated by two competing mechanisms, dimerization or SVSH, and the dominant pathway was largely determined by the polarization of thiol molecules and the temperature. It is also worth noting that the authors predicted that the Mo-H bond was formed in the dimerization mechanism which is different from the other report about the same mechanism.<sup>113,114</sup> In 2021, Zhang *et al.* directly monitored the interaction between the fluorescent thiol and SVs in a metal-organic chemical vapor deposition (MOCVD)-grown  $\text{MoS}_2$  monolayer *via* 2D point accumulation for imaging in a nanoscale topography (PAINT) strategy (Fig. 2w) and revealed a hydroxide-assisted transition from the reversible interaction (physisorption) to covalent binding by deprotonation of the thiol while increasing the pH.<sup>115</sup>

The SVs could also be passivated by the formation of a van der Waals interface, proposed as a physisorption mechanism like the use of ML TiOPc on the  $\text{MoS}_2$  surface.<sup>71</sup> Park *et al.* revealed a van der Waals interaction *via* scanning tunneling microscopy (STM) and DFT modeling, in which a negative charge transfer from  $\text{MoS}_2$  to TiOPc removes defect states.<sup>71</sup> As illustrated in Fig. 5d, it was hypothesized that a thermally stable TiOPc ML was formed on the  $\text{MoS}_2$  surface, which did not induce physical reconstructions of defects. Similarly, Ahn *et al.* reported that MPcs passivated SVs in ME  $\text{MoS}_2$ , evidenced by the weakened PL peak at 1.79 eV (associated with excitons bound to defects) after the treatment in low-temperature PL measurements.<sup>116,117</sup>

Besides organic thiol molecules and MPcs, there were other approaches reported for passivating defects in 2D TMDSS. Tapasztó and co-workers reported that the defects in  $\text{MoS}_2$  resulted from  $\text{O}_2$  oxidation, where  $\text{O}_2$  spontaneously incorporated into the basal plane of monolayer  $\text{MoS}_2$  during ambient exposure (Fig. 2v). The substitutional oxidation of  $\text{MoS}_2$  could be fully recovered to pristine *via* annealing the oxygen-substituted  $\text{MoS}_2$  under a  $\text{H}_2\text{S}$  atmosphere at  $200\text{ }^\circ\text{C}$ , which was evidenced by STM images and DFT calculations.<sup>118</sup> On the other hand, there were a few research groups that reported that the chemisorption of  $\text{O}_2$  could passivate the SVs of TMDSS and result in a defect-free electronic band structure similar to that of perfect monolayer TMDSS.<sup>64,101,119,120</sup> Sivaram *et al.* proposed that  $\text{H}_2\text{O}$  could passivate SVs in the CVD-grown  $\text{MoS}_2$ , but the reaction required photo-generated excitons to overcome a large absorption barrier (Fig. 4c).<sup>121</sup> The  $\text{H}_2\text{O}$  molecule was physisorbed on the surface of  $\text{MoS}_2$  using an empty anti-bonding orbital, then the exciton-mediated dissociation of

$\text{H}_2\text{O}$  resulted in the O atom bonded to the SV with a valency of  $-2$ , and the  $\text{H}_2$  molecule desorbed from the  $\text{MoS}_2$  surface.

### 3. Chemical passivation of $\text{MoSe}_2$ and $\text{WSe}_2$

#### 3.1 Characterization

To date, few general chemical treatments enhance the quality of both sulfur-based and selenide-based 2D TMD materials, which can be attributed to their different intrinsic doping levels and defects.<sup>81,91</sup> For instance, 2D  $\text{WSe}_2$  is known to be a p-type semiconductor while  $\text{MoSe}_2$  is known to be an n-type semiconductor due to its intrinsic defects.<sup>122,123</sup> In 2016, Javey and co-workers reported the effects of H-TFSI treatments on the PLQY of  $\text{MoS}_2$ ,  $\text{WS}_2$ ,  $\text{MoSe}_2$ , and  $\text{WSe}_2$ , and suggested that only the defects in sulfur-based 2D TMD materials were amenable to the H-TFSI treatment.<sup>124</sup>

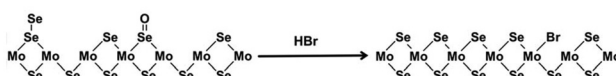


Fig. 6 Illustration of the chemical reaction on the surface of  $\text{MoSe}_2$  during the HBr treatment. This figure has been adapted from ref. 127 with permission from American Chemical Society, copyright 2015.

able to the H-TFSI treatment.<sup>124</sup> Later, they reported that ME  $\text{MoS}_2$  and  $\text{WSe}_2$  monolayers were hardly doped, and the electrostatic doping was, therefore, not able to enhance their emission.<sup>103</sup> This work bore some differences from a related study by Yu *et al.*, who reported a PL increase of the CVD as-grown  $\text{WSe}_2$  and  $\text{MoSe}_2$  monolayers after the H-TFSI treatment.<sup>96</sup> On the other hand, Ahn *et al.* reported that both n-type dopant zinc phthalocyanine (ZnPc) and p-type dopant zinc hexadecafluoro phthalocyanine ( $\text{F}_{16}\text{ZnPc}$ ) resulted in quenching of PL from CVD-grown few-layer  $\text{MoSe}_2$ .<sup>116</sup> In 2021, Rao and co-workers demonstrated that the OA treatment on ME  $\text{MoSe}_2$  monolayers enhanced the PL yield of  $\text{MoSe}_2$  by an average of 58-fold, while also improving the spectral uniformity of brightness and reducing the emission linewidth.<sup>125</sup> The authors revealed trap-free neutral exciton movement in OA-treated  $\text{MoSe}_2$  monolayers evidenced by steady-state excitation intensity-dependent PL and TRPL studies and thus postulated that the defect passivation scheme of the OA treatment was related to selenium vacancy passivation through oleate coordination to Mo dangling bonds without distinguishable structural changes. Recently, Deng and co-workers reported  $\text{MoSe}_2$  monolayers with lateral size  $>1$  mm with a uniformly high PLQY using 1-dodecanol encapsulation, which both passivated the chalcogen vacancies and suppressed substrate quenching of the excitons.<sup>126</sup>

Table 1 Summary of the reported literature data (main text) for the effect of chemical treatments on the PL of TMDs

Material (monolayer)	Exfoliation/synthesis method	Untreated			Treated					Ref.
		PL peak (eV)	QY (%)	PL lifetime (ns)	Chemical treatment	PL peak (eV)	$I^a$	QY (%)	PL lifetime (ns)	
$\text{MoS}_2$	ME	1.85	—	—	F4TCNQ	1.88	10	—	—	59 and 60
		1.87	—	—	$\text{H}_2\text{O}_2$	1.89	27.4	12	—	61
		1.84	—	—	$\text{O}_2, \text{H}_2\text{O}$ (after annealing)	1.88	100	—	—	62
		1.79	—	—	$\text{O}_2$ (after annealing)	1.83	30	—	—	64
		1.88	1	0.3	H-TFSI	1.88	190	95	10.8	67
		1.88	0.1–1	—	CYTOP + H-TFSI	1.88	>100	55–100	15	68
		1.88	—	<0.1	Thiols + H-TFSI	1.88	275	—	2.5	83
		1.86	—	—	MB	1.88	2	—	—	91
	CVD	1.87	—	<0.1	Li-TFSI	1.88	50	—	0.32	94
		~1.89	—	—	$\text{H}_2\text{SO}_4/\text{H}_2\text{O}_2$	~1.91	20	—	—	101
		1.89	—	—	IL	1.89	100	—	—	70
		1.84	—	—	TiOPc	1.85	3	—	—	71
$\text{WS}_2$	CVD/ME BE + LPE	1.86	—	—	PEDOT:PSS	1.88	2	—	—	72
		1.87	—	0.11	Methanol	1.86	2.2	—	0.15	81
		~1.85	—	—	H-TFSI/Li-TFSI	~1.91	>80	—	—	96
		1.89	0.1	—	H-TFSI	1.90	10	1.5–15	—	98
		1.85	—	—	$\text{H}_2\text{O} + h\nu$	1.85	200	—	—	121
		~1.81	—	—	Thiols	~1.82	~2	—	—	73
		—	<1	6.08	THF + heating	~2.66	64	18.5	4.67	75
		1.96	—	—	F4TCNQ	2.02	3	—	—	63
	CVD	2.01	—	0.06	OA	2.02	40	—	0.25	82
		2.01	—	—	$\text{Na}_2\text{S}$	1.96	25	—	—	74
		~1.88	—	—	H-TFSI/Li-TFSI	~2.0	>60	—	—	96
		1.94	—	—	H-TFSI	2.01	25	—	—	97
$\text{MoSe}_2$	CVD	~1.57	—	—	H-TFSI/Li-TFSI	~1.58	>10	—	—	96
		1.53	—	—	HBr	1.55	30	—	—	127
	ME	1.53	2.5	0.48	Ethanol	1.55	3.5	16	1.67	132
		1.56	—	1.07	OA	1.58	61	—	3.3	125
$\text{WSe}_2$	CVD	1.56	1	1	Acetone	1.65	~15	60	4.1	131

<sup>a</sup> PL intensity enhancement factor (times).



### 3.2 Mechanisms of chemical passivation

Han *et al.* reported that the HBr treatment enhanced the PL intensity of CVD-grown monolayer MoSe<sub>2</sub> more than 30 times through p-doping and defect healing.<sup>127</sup> The p-doping effect was validated by the intensity increase and frequency upshift of A<sub>1g</sub> mode in Raman spectroscopy. Undesired oxidized Se<sup>4+</sup> and bridging Se<sub>2</sub><sup>2-</sup> defects were removed, which was visualized by the peak shift and full width at half-maximum (FWHM) decrease of Mo<sup>(IV)</sup> 3d, as well as the elemental ratio increase of the anion to Mo in XPS spectra. The possible mechanism of HBr treatment proposed by the authors is illustrated in Fig. 6.

A few other molecules and treatment protocols have also been reported for passivating defects. Guo *et al.* proposed that the Se vacancies in MoSe<sub>2</sub> could be well passivated with halogen atoms (except F) using first-principles calculation, through a p-doping process.<sup>128</sup> Mahjouri-Samani *et al.* reported that the vaporization of selenium in a vacuum using a pulsed laser repaired Se vacancies in the synthesized MoSe<sub>2</sub>.<sup>129</sup> Lu *et al.* demonstrated the passivation of Se vacancies by oxygen through a focused laser treatment in air on CVD-grown WSe<sub>2</sub>, which was verified by an enhancement in the PL intensity, an improvement of the photoconductivity (~150 times), an increase of the W oxidation ratio in XPS, as well as an increase in thickness in AFM images.<sup>130</sup> Ahn *et al.* reported that metallophthalocyanines (MPcs) exhibited defect-healing effects on the surface of the CVD-grown MoSe<sub>2</sub> monolayer, evidenced by the temperature-dependent blueshift of the band gap, the narrower PL bandwidth, and the suppression of mid-gap defect-induced absorption in ultrafast pump-probe spectroscopy.<sup>116</sup>

Moreover, Javey and co-workers reported a PLQY of ~60% in CVD-grown WSe<sub>2</sub> monolayers after undergoing a solvent evaporation-mediated decoupling (SEMD) process, which was also higher than that in ME WSe<sub>2</sub> monolayers by an order of magnitude.<sup>131</sup> They attributed the enhanced PLQY to reduced nonradiative recombination due to the release of built-in strain by decoupling the grown WSe<sub>2</sub> monolayer during the SEMD process validated by electron diffraction, *in situ* PL imaging, TEM, and TRPL measurements. Similarly, Chen *et al.* demonstrated that the PLQYs of both MoS<sub>2</sub> and MoSe<sub>2</sub> were enhanced by the solvent with a moderate volatilization rate like ethanol.<sup>132</sup>

## 4. Conclusions and perspectives

This mini-review provides an overview of the state-of-the-art chemical treatments and related mechanisms on TMDs. The low quality of 2D TMD materials has been a veritable bottleneck to the incorporation of 2D TMDs in practical optoelectronic devices. Thus, we focus more on strategies to improve the intrinsic quality of TMDs by passivating atomic defects or reducing their inherent doping with surface chemical treatments and discuss the discrepancies of reported related mechanisms. The photoluminescence of monolayer TMDs and the mobility of FET devices built on 2D TMDs are

utilized as the two most important quality factors to evaluate the effect of chemical treatments. The PL and mobility of resulting FET devices have been hugely improved with varied surface chemical treatments in most cases. The mechanisms behind the chemical treatments have also been theoretically and experimentally explored for further development of chemical treatment approaches. We have thus tried to present the research to date on chemical treatments and the mechanisms behind them in this mini-review, and in some cases, the literature is converging on a unified picture. However, disagreement and discrepancies across different treatments and mechanisms remain. This must be resolved to move forward. A summary of the reported data for the effect of chemical treatments on the PL of TMDs can be found in Table 1. Since it is technically very difficult to measure the PLQY from 100 μm<sup>2</sup> monolayer flakes, the shape and position of the steady-state PL spectra also serve as a quality indicator of 2D TMDs both the PL intensity and PL shape of the same monolayer flakes before and after chemical treatment should be measured.<sup>133</sup> Moreover, as previously described, some of the discrepancies in disclosed mechanisms may be ascribed to the lack of comparison of various chemical treatments on TMD monolayers with the same synthesis method and under the same measurement conditions, as well as to the precision limit in characterization tools. Therefore, more attention should be paid to the synthesis of materials, and the experiments utilized for characterization should be carefully chosen and scrutinized to determine what can provide the most useful information for determining mechanisms. For instance, electrical transport measurements were utilized to support the defects passivation mechanism with enhanced mobility after chemical treatments, whereas the resulting mobilities were often limited by the contact between the monolayers and the electrodes, and chemicals like H-TFSI could corrode the contact, which led to an unfair comparison among various chemicals. From our perspective, an essential tool to characterize the effect of chemical treatments on 2D TMD materials is ultrafast spectroscopy, which can reveal the carrier dynamics associated with defects without the additional complications of contacts and electrodes. However, this should not be performed in isolation, as the variation of exciton dynamics associated with defects and doping renders multiple processes with a variety of time scales that can also overlap.<sup>134</sup> Advanced microscopy techniques such as cavity-enhanced extinction microscopy and single-molecule localization microscopy coupled with fluorescence labelling are reported to give new insights into the defects' properties of 2D materials.<sup>115,135</sup> Therefore, we contend that the most robust approach is to combine various experimental approaches to construct a hypothesis.

Other challenges must be addressed to take full advantage of 2D TMDs in practical optoelectronic applications. For instance, another area we identify for specific future work and possible commercialization is the improvement of liquid exfoliation (LE) of 2D TMDs.<sup>85,136</sup> Although the LE methodology and the quality of liquid-exfoliated TMD nanosheets have been developed and improved constantly, the PLQY of liquid-exfo-



liated TMD nanosheets remains an outstanding challenge, which limits the scalability of device application to a large extent.<sup>44,137–140</sup> Chemical treatment development towards being compatible with the liquid exfoliation process could be extremely fruitful for possible applications in flexible optoelectronics.

## Author contributions

Z. Li conceived the idea and wrote the paper with input from H. Bretscher and A. Rao. All authors contributed to the organization of the content.

## Conflicts of interest

There are no conflicts to declare.

## Acknowledgements

A. R. is grateful for the invitation to this contribution from the editor office. We acknowledge funding from the Swedish Research Council, Vetenskapsrådet 2018-06610, and ÅForsk Foundation nr. 22-390.

## References

- 1 K. S. Novoselov, V. I. Fal'Ko, L. Colombo, P. R. Gellert, M. G. Schwab and K. Kim, *Nature*, 2012, **490**, 192–200.
- 2 C. Tan, X. Cao, X. J. Wu, Q. He, J. Yang, X. Zhang, J. Chen, W. Zhao, S. Han, G. H. Nam, M. Sindoro and H. Zhang, *Chem. Rev.*, 2017, **117**, 6225–6331.
- 3 T. D. Thanh, N. D. Chuong, H. Van Hien, T. Kshetri, L. H. Tuan, N. H. Kim and J. H. Lee, *Prog. Mater. Sci.*, 2018, **96**, 51–85.
- 4 X. Li, L. Tao, Z. Chen, H. Fang, X. Li, X. Wang, J. Bin Xu and H. Zhu, *Appl. Phys. Rev.*, 2017, **4**, 021306.
- 5 A. Hirsch and F. Hauke, *Angew. Chem., Int. Ed.*, 2018, **57**, 4338–4354.
- 6 F. Yan, Z. Wei, X. Wei, Q. Lv, W. Zhu and K. Wang, *Small Methods*, 2018, **2**, 1–14.
- 7 K. F. Mak and J. Shan, *Nat. Photonics*, 2016, **10**, 216–226.
- 8 A. Krasnok, S. Lepeshov and A. Alú, *Opt. Express*, 2018, **26**, 15972.
- 9 D. Jariwala, V. K. Sangwan, L. J. Lauhon, T. J. Marks and M. C. Hersam, *ACS Nano*, 2014, **8**, 1102–1120.
- 10 W. Zheng, Y. Jiang, X. Hu, H. Li, Z. Zeng, X. Wang and A. Pan, *Adv. Opt. Mater.*, 2018, **6**, 1–29.
- 11 K. F. Mak, C. Lee, J. Hone, J. Shan and T. F. Heinz, *Phys. Rev. Lett.*, 2010, **105**, 2–5.
- 12 J. Shim, H. Y. Park, D. H. Kang, J. O. Kim, S. H. Jo, Y. Park and J. H. Park, *Adv. Electron. Mater.*, 2017, **3**, 1600364.
- 13 J. Kim, S. Zhang, S. Hou, B. Lee, G. Wei and S. R. Forrest, *ACS Photonics*, 2021, **8**, 1152–1158.
- 14 J. W. T. Seo, J. Zhu, V. K. Sangwan, E. B. Secor, S. G. Wallace and M. C. Hersam, *ACS Appl. Mater. Interfaces*, 2019, **11**, 5675–5681.
- 15 Y. Cui, Z. Zhou, T. Li, K. Wang, J. Li and Z. Wei, *Adv. Funct. Mater.*, 2019, **29**, 1–33.
- 16 Y. Liu, X. Duan, H. J. Shin, S. Park, Y. Huang and X. Duan, *Nature*, 2021, **591**, 43–53.
- 17 Z. Cheng, R. Cao, K. Wei, Y. Yao, X. Liu, J. Kang, J. Dong, Z. Shi, H. Zhang and X. Zhang, *Adv. Sci.*, 2021, **8**, 1–22.
- 18 K. Nassiri Nazif, A. Daus, J. Hong, N. Lee, S. Vaziri, A. Kumar, F. Nitta, M. E. Chen, S. Kananian, R. Islam, K.-H. Kim, J.-H. Park, A. S. Y. Poon, M. L. Brongersma, E. Pop and K. C. Saraswat, *Nat. Commun.*, 2021, **12**, 7034.
- 19 D. Rhodes, S. H. Chae, R. Ribeiro-Palau and J. Hone, *Nat. Mater.*, 2019, **18**, 541–549.
- 20 A. Chernikov, T. C. Berkelbach, H. M. Hill, A. Rigosi, Y. Li, O. B. Aslan, D. R. Reichman, M. S. Hybertsen and T. F. Heinz, *Phys. Rev. Lett.*, 2014, **113**, 1–5.
- 21 Y. You, X. X. Zhang, T. C. Berkelbach, M. S. Hybertsen, D. R. Reichman and T. F. Heinz, *Nat. Phys.*, 2015, **11**, 477–481.
- 22 Z. Ye, T. Cao, K. O'Brien, H. Zhu, X. Yin, Y. Wang, S. G. Louie and X. Zhang, *Nature*, 2014, **513**, 214–218.
- 23 M. M. Ugeda, A. J. Bradley, S. F. Shi, F. H. Da Jornada, Y. Zhang, D. Y. Qiu, W. Ruan, S. K. Mo, Z. Hussain, Z. X. Shen, F. Wang, S. G. Louie and M. F. Crommie, *Nat. Mater.*, 2014, **13**, 1091–1095.
- 24 K. F. Mak, K. He, C. Lee, G. H. Lee, J. Hone, T. F. Heinz and J. Shan, *Nat. Mater.*, 2013, **12**, 207–211.
- 25 J. Pető, T. Ollár, P. Vancsó, Z. I. Popov, G. Z. Magda, G. Dobrik, C. Hwang, P. B. Sorokin and L. Tapasztó, *Nat. Chem.*, 2018, **10**, 1246–1251.
- 26 N. Kang, H. P. Paudel, M. N. Leuenberger, L. Tetard and S. I. Khondaker, *J. Phys. Chem. C*, 2014, **118**, 21258–21263.
- 27 B. G. Shin, G. H. Han, S. J. Yun, H. M. Oh, J. J. Bae, Y. J. Song, C. Y. Park and Y. H. Lee, *Adv. Mater.*, 2016, **28**, 9378–9384.
- 28 X. Zou and B. I. Yakobson, *Acc. Chem. Res.*, 2015, **48**, 73–80.
- 29 S. Haldar, H. Vovusha, M. K. Yadav, O. Eriksson and B. Sanyal, *Phys. Rev. B: Condens. Matter Mater. Phys.*, 2015, **92**, 1–12.
- 30 H. Liu, N. Han and J. Zhao, *RSC Adv.*, 2015, **5**, 17572–17581.
- 31 J. A. Robinson and B. Schuler, *Appl. Phys. Lett.*, 2021, **119**, 140501.
- 32 S. M. Hus and A. P. Li, *Prog. Surf. Sci.*, 2017, **92**, 176–201.
- 33 S. Y. Seo, D. H. Yang, G. Moon, O. F. N. Okello, M. Y. Park, S. H. Lee, S. Y. Choi and M. H. Jo, *Nano Lett.*, 2021, **21**, 3341–3354.
- 34 Q. Zhang, A. T. S. Wee, Q. Liang, X. Zhao and M. Liu, *ACS Nano*, 2021, **15**, 2165–2181.
- 35 Y. Yu, Y. Yu, C. Xu, Y. Q. Cai, L. Su, Y. Zhang, Y. W. Zhang, K. Gundogdu and L. Cao, *Adv. Funct. Mater.*, 2016, **26**, 4733–4739.



36 O. A. Ajayi, J. V. Ardelean, G. D. Shepard, J. Wang, A. Antony, T. Taniguchi, K. Watanabe, T. F. Heinz, S. Strauf, X. Y. Zhu and J. C. Hone, *2D Mater.*, 2016, **26**, 4733–4739.

37 F. Cadiz, E. Courtade, C. Robert, G. Wang, Y. Shen, H. Cai, T. Taniguchi, K. Watanabe, H. Carrere, D. Lagarde, M. Manca, T. Amand, P. Renucci, S. Tongay, X. Marie and B. Urbaszek, *Phys. Rev. X*, 2017, **7**, 1–12.

38 Z. Liu, M. Amani, S. Najmaei, Q. Xu, X. Zou, W. Zhou, T. Yu, C. Qiu, A. G. Birdwell, F. J. Crowne, R. Vajtai, B. I. Yakobson, Z. Xia, M. Dubey, P. M. Ajayan and J. Lou, *Nat. Commun.*, 2014, **5**, 5246.

39 Z. Li, Y. Lv, L. Ren, J. Li, L. Kong, Y. Zeng, Q. Tao, R. Wu, H. Ma, B. Zhao, D. Wang, W. Dang, K. Chen, L. Liao, X. Duan, X. Duan and Y. Liu, *Nat. Commun.*, 2020, **11**, 1–8.

40 H. H. Huang, X. Fan, D. J. Singh and W. T. Zheng, *Nanoscale*, 2020, **12**, 1247–1268.

41 R. Wang, Y. Yu, S. Zhou, H. Li, H. Wong, Z. Luo, L. Gan and T. Zhai, *Adv. Funct. Mater.*, 2018, **28**, 1802473.

42 S. Bertolazzi, M. Gobbi, Y. Zhao, C. Backes and P. Samorì, *Chem. Soc. Rev.*, 2018, **47**, 6845–6888.

43 K. Cho, J. Pak, S. Chung and T. Lee, *ACS Nano*, 2019, **13**, 9713–9734.

44 S. Ippolito, A. Ciesielski and P. Samorì, *Chem. Commun.*, 2019, **55**, 8900–8914.

45 L. Huang, A. Krasnok, A. Alu, Y. Yu, D. Neshev and A. E. Miroshnichenko, *Rep. Prog. Phys.*, 2022, **85**, 046401.

46 X. Dai, Z. Yang, A. Li, J. Yang and F. Ouyang, *Superlattices Microstruct.*, 2019, **130**, 528–538.

47 J. Zhou, F. Liu, J. Lin, X. Huang, J. Xia, B. Zhang, Q. Zeng, H. Wang, C. Zhu, L. Niu, X. Wang, W. Fu, P. Yu, T. R. Chang, C. H. Hsu, D. Wu, H. T. Jeng, Y. Huang, H. Lin, Z. Shen, C. Yang, L. Lu, K. Suenaga, W. Zhou, S. T. Pantelides, G. Liu and Z. Liu, *Adv. Mater.*, 2017, **29**, 1603471.

48 D. Qu, X. Liu, M. Huang, C. Lee, F. Ahmed, H. Kim, R. S. Ruoff, J. Hone and W. J. Yoo, *Adv. Mater.*, 2017, **29**, 1–11.

49 J. Hong, Z. Hu, M. Probert, K. Li, D. Lv, X. Yang, L. Gu, N. Mao, Q. Feng, L. Xie, J. Zhang, D. Wu, Z. Zhang, C. Jin, W. Ji, X. Zhang, J. Yuan and Z. Zhang, *Nat. Commun.*, 2015, **6**, 1–8.

50 X. Zou, Y. Liu and B. I. Yakobson, *Nano Lett.*, 2013, **13**, 253–258.

51 S. Najmaei, Z. Liu, W. Zhou, X. Zou, G. Shi, S. Lei, B. I. Yakobson, J. C. Idrobo, P. M. Ajayan and J. Lou, *Nat. Mater.*, 2013, **12**, 754–759.

52 V. Carozo, Y. Wang, K. Fujisawa, B. R. Carvalho, A. McCreary, S. Feng, Z. Lin, C. Zhou, N. Perea-López, A. L. Elías, B. Kabius, V. H. Crespi and M. Terrones, *Sci. Adv.*, 2017, **3**, 1–10.

53 W. Bao, N. J. Borys, C. Ko, J. Suh, W. Fan, A. Thron, Y. Zhang, A. Buyanin, J. Zhang, S. Cabrini, P. D. Ashby, A. Weber-Bargioni, S. Tongay, S. Aloni, D. F. Ogletree, J. Wu, M. B. Salmeron and P. J. Schuck, *Nat. Commun.*, 2015, **6**, 1–7.

54 W. Su, L. Jin, X. Qu, D. Huo and L. Yang, *Phys. Chem. Chem. Phys.*, 2016, **18**, 14001–14006.

55 S. Barja, S. Refaeli-Abramson, B. Schuler, D. Y. Qiu, A. Pulkin, S. Wickenburg, H. Ryu, M. M. Ugeda, C. Kastl, C. Chen, C. Hwang, A. Schwartzberg, S. Aloni, S. K. Mo, D. Frank Ogletree, M. F. Crommie, O. V. Yazyev, S. G. Louie, J. B. Neaton and A. Weber-Bargioni, *Nat. Commun.*, 2019, **10**, 1–8.

56 J. D. Lin, C. Han, F. Wang, R. Wang, D. Xiang, S. Qin, X. A. Zhang, L. Wang, H. Zhang, A. T. S. Wee and W. Chen, *ACS Nano*, 2014, **8**, 5323–5329.

57 M. Tebyetekerwa, J. Zhang, Z. Xu, T. N. Truong, Z. Yin, Y. Lu, S. Ramakrishna, D. Macdonald and H. T. Nguyen, *ACS Nano*, 2020, **14**, 14579–14604.

58 Y. Zhu, J. Lim, Z. Zhang, Y. Wang, S. Sarkar, H. Ramsden, Y. Li, H. Yan, D. Phuyal, N. Gauriot, A. Rao, R. L. Z. Hoye, G. Eda and M. Chhowalla, *ACS Nano*, 2023, **17**, 13545–13553.

59 S. Mouri, Y. Miyauchi and K. Matsuda, *Nano Lett.*, 2013, **13**, 5944–5948.

60 S. Mouri, Y. Miyauchi and K. Matsuda, *Appl. Phys. Express*, 2016, **9**, 1–4.

61 W. Su, H. Dou, J. Li, D. Huo, N. Dai and L. Yang, *RSC Adv.*, 2015, **5**, 82924–82929.

62 S. Tongay, J. Zhou, C. Ataca, J. Liu, J. S. Kang, T. S. Matthews, L. You, J. Li, J. C. Grossman and J. Wu, *Nano Lett.*, 2013, **13**, 2831–2836.

63 N. Peimyoo, W. Yang, J. Shang, X. Shen, Y. Wang and T. Yu, *ACS Nano*, 2014, **8**, 11320–11329.

64 H. Nan, Z. Wang, W. Wang, Z. Liang, Y. Lu, Q. Chen, D. He, P. Tan, F. Miao, X. Wang, J. Wang and Z. Ni, *ACS Nano*, 2014, **8**, 5738–5745.

65 L. Sun, X. Zhang, F. Liu, Y. Shen, X. Fan, S. Zheng, J. T. L. Thong, Z. Liu, S. A. Yang and H. Y. Yang, *Sci. Rep.*, 2017, **7**, 1–9.

66 L. Xu, L. Zhao, Y. Wang, M. Zou, Q. Zhang and A. Cao, *Nano Res.*, 2019, **12**, 1619–1624.

67 M. Amani, D. H. Lien, D. Kiriya, J. Xiao, A. Azcatl, J. Noh, S. R. Madhvapathy, R. Addou, K. C. Santosh, M. Dubey, K. Cho, R. M. Wallace, S. C. Lee, J. H. He, J. W. Ager, X. Zhang, E. Yablonovitch and A. Javey, *Science*, 2015, **350**, 1065–1068.

68 H. Kim, D. H. Lien, M. Amani, J. W. Ager and A. Javey, *ACS Nano*, 2017, **11**, 5179–5185.

69 A. J. Goodman, A. P. Willard and W. A. Tisdale, *Phys. Rev. B*, 2017, **96**, 1–6.

70 T. L. Atallah, J. Wang, M. Bosch, D. Seo, R. A. Burke, O. Moneer, J. Zhu, M. Theibault, L. E. Brus, J. Hone and X. Y. Zhu, *J. Phys. Chem. Lett.*, 2017, **8**, 2148–2152.

71 J. H. Park, A. Sanne, Y. Guo, M. Amani, K. Zhang, H. C. P. Mowva, J. A. Robinson, A. Javey, J. Robertson, S. K. Banerjee and A. C. Kummel, *Sci. Adv.*, 2017, **3**, 1–7.

72 X. Zhang, Q. Liao, S. Liu, Z. Kang, Z. Zhang, J. Du, F. Li, S. Zhang, J. Xiao, B. Liu, Y. Ou, X. Liu, L. Gu and Y. Zhang, *Nat. Commun.*, 2017, **8**, 1–8.



73 Q. Ding, K. J. Czech, Y. Zhao, J. Zhai, R. J. Hamers, J. C. Wright and S. Jin, *ACS Appl. Mater. Interfaces*, 2017, **9**, 12734–12742.

74 H. Yao, L. Liu, Z. Wang, H. Li, L. Chen, M. E. Pam, W. Chen, H. Y. Yang, W. Zhang and Y. Shi, *Nanoscale*, 2018, **10**, 6105–6112.

75 Z. Li, Z. Chen, L. Xiao, X. Zhou, C. Zhao and Y. Zhang, *ACS Appl. Mater. Interfaces*, 2024, **16**, 15487–15495.

76 M. Y. Chan, K. Komatsu, S. L. Li, Y. Xu, P. Darmawan, H. Kuramochi, S. Nakaharai, A. Aparecido-Ferreira, K. Watanabe, T. Taniguchi and K. Tsukagoshi, *Nanoscale*, 2013, **5**, 9572–9576.

77 S. Najmaei, X. Zou, D. Er, J. Li, Z. Jin, W. Gao, Q. Zhang, S. Park, L. Ge, S. Lei, J. Kono, V. B. Shenoy, B. I. Yakobson, A. George, P. M. Ajayan and J. Lou, *Nano Lett.*, 2014, **14**, 1354–1361.

78 D. Lim, E. S. Kannan, I. Lee, S. Rathi, L. Li, Y. Lee, M. A. Khan, M. Kang, J. Park and G. H. Kim, *Nanotechnology*, 2016, **27**, 225201.

79 B. Radisavljevic, A. Radenovic, J. Brivio, V. Giacometti and A. Kis, *Nat. Nanotechnol.*, 2011, **6**, 147–150.

80 Z. Yu, Y. Pan, Y. Shen, Z. Wang, Z. Y. Ong, T. Xu, R. Xin, L. Pan, B. Wang, L. Sun, J. Wang, G. Zhang, Y. W. Zhang, Y. Shi and X. Wang, *Nat. Commun.*, 2014, **5**, 1–7.

81 G. P. Neupane, M. D. Tran, S. J. Yun, H. Kim, C. Seo, J. Lee, G. H. Han, A. K. Sood and J. Kim, *ACS Appl. Mater. Interfaces*, 2017, **9**, 11950–11958.

82 A. O. A. Tanoh, J. Alexander-Webber, J. Xiao, G. Delport, C. A. Williams, H. Bretscher, N. Gauriot, J. Allardice, R. Pandya, Y. Fan, Z. Li, S. Vignolini, S. D. Stranks, S. Hofmann and A. Rao, *Nano Lett.*, 2019, **19**, 6299–6307.

83 H. Bretscher, Z. Li, J. Xiao, D. Y. Qiu, S. Refaelly-Abramson, J. A. Alexander-Webber, A. Tanoh, Y. Fan, G. Delport, C. A. Williams, S. D. Stranks, S. Hofmann, J. B. Neaton, S. G. Louie and A. Rao, *ACS Nano*, 2021, **15**, 8780–8789.

84 S. Ippolito, A. G. Kelly, R. Furlan de Oliveira, M. A. Stoeckel, D. Iglesias, A. Roy, C. Downing, Z. Bian, L. Lombardi, Y. A. Samad, V. Nicolosi, A. C. Ferrari, J. N. Coleman and P. Samori, *Nat. Nanotechnol.*, 2021, **16**, 592–598.

85 S. Ippolito, F. Urban, W. Zheng, O. Mazzarisi, C. Valentini, A. G. Kelly, S. M. Gali, M. Bonn, D. Beljonne, F. Corberi, J. N. Coleman, H. I. Wang and P. Samori, *Adv. Mater.*, 2023, 2211157.

86 E. P. Nguyen, B. J. Carey, J. Z. Ou, J. Van Embden, E. Della Gaspera, A. F. Chrimes, M. J. S. Spencer, S. Zhuiykov, K. Kalantar-Zadeh and T. Daeneke, *Adv. Mater.*, 2015, **27**, 6225–6229.

87 D. Pierucci, H. Henck, Z. Ben Aziza, C. H. Naylor, A. Balan, J. E. Rault, M. G. Silly, Y. J. Dappe, F. Bertran, P. Le Fèvre, F. Sirotti, A. T. C. Johnson and A. Ouerghi, *ACS Nano*, 2017, **11**, 1755–1761.

88 D. M. Sim, M. Kim, S. Yim, M. J. Choi, J. Choi, S. Yoo and Y. S. Jung, *ACS Nano*, 2015, **9**, 12115–12123.

89 S. H. Amsterdam, T. K. Stanev, L. Wang, Q. Zhou, S. Irgen-Giorgio, S. Padgaonkar, A. A. Murthy, V. K. Sangwan, V. P. Dravid, E. A. Weiss, P. Darancet, M. K. Y. Chan, M. C. Hersam, N. P. Stern and T. J. Marks, *J. Am. Chem. Soc.*, 2021, **143**, 17153–17161.

90 A. Tarasov, S. Zhang, M. Y. Tsai, P. M. Campbell, S. Graham, S. Barlow, S. R. Marder and E. M. Vogel, *Adv. Mater.*, 2015, **27**, 1175–1181.

91 S. Zhang, H. M. Hill, K. Moudgil, C. A. Richter, A. R. Hight Walker, S. Barlow, S. R. Marder, C. A. Hacker and S. J. Pookpanratana, *Adv. Mater.*, 2015, **27**, 02991.

92 B. Birmingham, J. Yuan, M. Filez, D. Fu, J. Hu, J. Lou, M. O. Scully, B. M. Weckhuysen and Z. Zhang, *J. Phys. Chem. C*, 2019, **123**, 15738–15743.

93 Y. Wang, A. Slassi, M. A. Stoeckel, S. Bertolazzi, J. Cornil, D. Beljonne and P. Samori, *J. Phys. Chem. Lett.*, 2019, **10**, 540–547.

94 Z. Li, H. Bretscher, Y. Zhang, G. Delport, J. Xiao, A. Lee, S. D. Stranks and A. Rao, *Nat. Commun.*, 2021, **12**, 6044.

95 Z. Li, D. Li, H. Wang, X. Xu, L. Pi, P. Chen, T. Zhai and X. Zhou, *ACS Nano*, 2022, **16**, 4884–4891.

96 Y. Yu, G. Li, L. Huang, A. Barrette, Y. Q. Cai, Y. Yu, K. Gundogdu, Y. W. Zhang and L. Cao, *ACS Nano*, 2017, **11**, 9390–9396.

97 K. P. Dhakal, S. Roy, S. J. Yun, G. Ghimire, C. Seo and J. Kim, *J. Mater. Chem. C*, 2017, **5**, 6820–6827.

98 S. Roy, W. Choi, S. Jeon, D. H. Kim, H. Kim, S. J. Yun, Y. Lee, J. Lee, Y. M. Kim and J. Kim, *Nano Lett.*, 2018, **18**, 4523–4530.

99 D. Kiriya, Y. Hijikata, J. Pirillo, R. Kitaura, A. Murai, A. Ashida, T. Yoshimura and N. Fujimura, *Langmuir*, 2018, **34**, 10243–10249.

100 H. Lu, A. Kummel and J. Robertson, *APL Mater.*, 2018, **6**, 066104.

101 C. Schwermann, T. Stiehm, P. Tonndorf, R. Schneider, R. Schmidt, J. Kern, S. Michaelis De Vasconcellos, R. Bratschitsch and N. L. Doltsinis, *Phys. Chem. Chem. Phys.*, 2018, **20**, 16918–16923.

102 M. R. Molas, K. Gołasa, L. Bala, K. Nogajewski, M. Bartos, M. Potemski and A. Babiński, *Sci. Rep.*, 2019, **9**, 1–7.

103 D. H. Lien, S. Z. Uddin, M. Yeh, M. Amani, H. Kim, J. W. Ager, E. Yablonovitch and A. Javey, *Science*, 2019, **364**, 468–471.

104 S. L. Pain, N. E. Grant and J. D. Murphy, *ACS Nano*, 2022, **16**, 1260–1270.

105 C. G. Wiegenstein and K. H. Schulz, *J. Phys. Chem. B*, 1999, **103**, 6913–6918.

106 M. Makarova, Y. Okawa and M. Aono, *J. Phys. Chem. C*, 2012, **116**, 22411–22416.

107 J. Y. Noh, H. Kim and Y. S. Kim, *Phys. Rev. B: Condens. Matter Mater. Phys.*, 2014, **89**, 1–12.

108 S. S. Chou, M. De, J. Kim, S. Byun, C. Dykstra, J. Yu, J. Huang and V. P. Dravid, *J. Am. Chem. Soc.*, 2013, **135**, 4584–4587.

109 J. S. Kim, H. W. Yoo, H. O. Choi and H. T. Jung, *Nano Lett.*, 2014, **14**, 5941–5947.

110 S. Karunakaran, S. Pandit, B. Basu and M. De, *J. Am. Chem. Soc.*, 2018, **140**, 12634–12644.



111 K. Cho, M. Min, T. Y. Kim, H. Jeong, J. Pak, J. K. Kim, J. Jang, S. J. Yun, Y. H. Lee, W. K. Hong and T. Lee, *ACS Nano*, 2015, **9**, 8044–8053.

112 X. Chen, N. C. Berner, C. Backes, G. S. Duesberg and A. R. McDonald, *Angew. Chem., Int. Ed.*, 2016, **55**, 5803–5808.

113 X. Chen, C. McGlynn and A. R. McDonald, *Chem. Mater.*, 2018, **30**, 6978–6982.

114 Q. Li, Y. Zhao, C. Ling, S. Yuan, Q. Chen and J. Wang, *Angew. Chem., Int. Ed.*, 2017, **56**, 10501–10505.

115 M. Zhang, M. Lihter, T. H. Chen, M. Macha, A. Rayabharam, K. Banjac, Y. Zhao, Z. Wang, J. Zhang, J. Comtet, N. R. Aluru, M. Lingenfelder, A. Kis and A. Radenovic, *ACS Nano*, 2021, **15**, 7168–7178.

116 H. Ahn, Y. C. Huang, C. W. Lin, Y. L. Chiu, E. C. Lin, Y. Y. Lai and Y. H. Lee, *ACS Appl. Mater. Interfaces*, 2018, **10**, 29145–29152.

117 S. Tongay, J. Suh, C. Ataca, W. Fan, A. Luce, J. S. Kang, J. Liu, C. Ko, R. Raghunathanan, J. Zhou, F. Ogletree, J. Li, J. C. Grossman and J. Wu, *Sci. Rep.*, 2013, **3**, 1–5.

118 J. Pető, T. Ollár, P. Vancsó, Z. I. Popov, G. Z. Magda, G. Dobrik, C. Hwang, P. B. Sorokin and L. Tapasztó, *Nat. Chem.*, 2018, **10**, 1246–1251.

119 B. Akdim, R. Pachter and S. Mou, *Nanotechnology*, 2016, **27**, 185701.

120 Y. Liu, P. Stradins and S. Wei, *Angew. Chem.*, 2016, **128**, 977–980.

121 S. V. Sivaram, A. T. Hanbicki, M. R. Rosenberger, G. G. Jernigan, H. J. Chuang, K. M. McCreary and B. T. Jonker, *ACS Appl. Mater. Interfaces*, 2019, **11**, 16147–16155.

122 M. Y. Tsai, S. Zhang, P. M. Campbell, R. R. Dasari, X. Ba, A. Tarasov, S. Graham, S. Barlow, S. R. Marder and E. M. Vogel, *Chem. Mater.*, 2017, **29**, 7296–7304.

123 L. C. Upadhyayula, J. J. Loferski, A. Wold, W. Giriat and R. Kershaw, *J. Appl. Phys.*, 1968, **39**, 4736–4740.

124 M. Amani, P. Taheri, R. Addou, G. H. Ahn, D. Kiriya, D. H. Lien, J. W. Ager, R. M. Wallace and A. Javey, *Nano Lett.*, 2016, **16**, 2786–2791.

125 A. O. A. Tanoh, J. Alexander-Webber, Y. Fan, N. Gauriot, J. Xiao, R. Pandya, Z. Li, S. Hofmann and A. Rao, *Nanoscale Adv.*, 2021, **3**, 4216–4225.

126 Q. Li, A. Alfrey, J. Hu, N. Lydick, E. Paik, B. Liu, H. Sun, Y. Lu, R. Wang, S. Forrest and H. Deng, *Nat. Commun.*, 2023, **14**, 1837.

127 H. V. Han, A. Y. Lu, L. S. Lu, J. K. Huang, H. Li, C. L. Hsu, Y. C. Lin, M. H. Chiu, K. Suenaga, C. W. Chu, H. C. Kuo, W. H. Chang, L. J. Li and Y. Shi, *ACS Nano*, 2016, **10**, 1454–1461.

128 Y. Guo, Y. Ji, H. Dong, L. Wang and Y. Li, *AIP Adv.*, 2019, **9**, 025202.

129 M. Mahjouri-Samani, L. Liang, A. Oyedele, Y. S. Kim, M. Tian, N. Cross, K. Wang, M. W. Lin, A. Boulesbaa, C. M. Rouleau, A. A. Puretzky, K. Xiao, M. Yoon, G. Eres, G. Duscher, B. G. Sumpter and D. B. Geohegan, *Nano Lett.*, 2016, **16**, 5213–5220.

130 J. Lu, A. Carvalho, X. K. Chan, H. Liu, B. Liu, E. S. Tok, K. P. Loh, A. H. Castro Neto and C. H. Sow, *Nano Lett.*, 2015, **15**, 3524–3532.

131 H. Kim, G. H. Ahn, J. Cho, M. Amani, J. P. Mastandrea, C. K. Groschner, D. H. Lien, Y. Zhao, J. W. Ager, M. C. Scott, D. C. Chrzan and A. Javey, *Sci. Adv.*, 2019, **5**, 1–8.

132 K. Chen, S. Deng, E. Chen, S. Wen, T. Ouyang, X. Wang, R. Zhan, J. Cai, X. Wan and H. Chen, *ACS Appl. Mater. Interfaces*, 2021, **13**, 44814–44823.

133 M. Tebyetekerwa, J. Zhang, Z. Xu, T. N. Truong, Z. Yin, Y. Lu, S. Ramakrishna, D. Macdonald and H. T. Nguyen, *ACS Nano*, 2020, **14**, 14579–14604.

134 L. Gao, Z. Hu, J. Lu, H. Liu and Z. Ni, *Phys. Chem. Chem. Phys.*, 2021, **23**, 8222–8235.

135 F. Sigger, I. Amersdorffer, A. Hötger, M. Nutz, J. Kiemele, T. Taniguchi, K. Watanabe, M. Förg, J. Noe, J. J. Finley, A. Högele, A. W. Holleitner, T. Hümmer, D. Hunger and C. Kastl, *J. Phys. Chem. Lett.*, 2022, **13**, 10291–10296.

136 Z. Li, F. Rashvand, H. Bretscher, B. M. Szydłowska, J. Xiao, C. Backes and A. Rao, *J. Phys. Chem. C*, 2022, **126**, 21681–21688.

137 C. Backes, B. M. Szydłowska, A. Harvey, S. Yuan, V. Vega-Mayoral, B. R. Davies, P. L. Zhao, D. Hanlon, E. J. G. Santos, M. I. Katsnelson, W. J. Blau, C. Gadermaier and J. N. Coleman, *ACS Nano*, 2016, **10**, 1589–1601.

138 S. Witomska, T. Leydecker, A. Ciesielski and P. Samorì, *Adv. Funct. Mater.*, 2019, **29**, 1–23.

139 F. Bonaccorso, A. Bartolotta, J. N. Coleman and C. Backes, *Adv. Mater.*, 2016, **28**, 6136–6166.

140 A. G. Kelly, V. Vega-Mayoral, J. B. Boland and J. N. Coleman, *2D Mater.*, 2019, **6**, 045036.

